First-order reversal-curve diagrams and reversible magnetization

C. R. Pike
Department of Geology, The University of California, Davis, California 95616, USA
(Received 10 June 2003; revised manuscript received 30 July 2003; published 22 September 2003)

First-order reversal curve (FORC) diagrams have recently been used for the characterization of magnetic systems in both geology and physics. However, the FORC distribution involves a mixed second derivative which reduces the reversible component of the magnetization to zero. As a result, the FORC distribution is not properly normalized. Furthermore, the calculation of the FORC distribution becomes unreliable near the axis where the reversible magnetization should be located (i.e., the $H=H_r$ axis). We propose here a method of incorporating the reversible magnetization into the FORC distribution using ''extended'' FORC's. With extended FORC's, the FORC distribution is properly normalized and robust near the $H=H_r$ axis.

DOI: 10.1103/PhysRevB.68.104424 PACS number(s): 75.60.Ej

I. INTRODUCTION

First-order reversal curve (FORC) diagrams[1] have been a topic of recent interest in both physics and geology.[2–5] A FORC diagram provides a detailed characterization of the hysteretic response of a magnetic system to an applied field. FORC diagrams are based on the procedure described by Mayergoyz for identifying the Preisach distribution of a classical Preisach system.[6] But with FORC diagrams, we perform this same procedure on all types of magnetic systems, regardless of whether or not they are classical Preisach systems, and we simply treat this procedure as a type of measurement.

A FORC diagram is generated from a class of minor hysteresis loops referred to as First-order reversal curves. As shown in Fig. 1, the acquisition of a FORC begins by saturating a system in a positive applied field. The applied field is lowered to a reversal field H_r, and a FORC is the magnetization curve that results when the field is increased back to saturation.[6] The magnetization at the applied field H on the FORC with reversal field H_r is denoted by $M(H,H_r)$, where $H \geqslant H_r$. A FORC distribution is defined as

$$\rho(H,H_r) \equiv -\frac{1}{2}\frac{\partial^2 M(H,H_r)}{\partial H_r \partial H}. \tag{1}$$

There can be regions where $\rho(H,H_r)$ is negative, so when we call $\rho(H,H_r)$ a distribution, we are generalizing the term ''distribution'' to include negative values. A contour plot of the FORC distribution is referred to as a FORC diagram.

The objective of this paper is to resolve three related issues in the definition and measurement of a FORC diagram. These issues involve (i) the normalization of the distribution, (ii) the representation of reversible magnetization on a FORC diagram, and (iii) the calculation of the FORC distribution near the $H=H_r$ axis.

II. EXTENDED DATASETS

The FORC distribution defined by Eq. 1 presents a problem involving normalization. Let us assume that as H goes to infinity, the magnetization M approaches a finite saturation value M_s. Then we would like $\rho(H,H_r)$ to be normalized, so that

$$\int \int_{H_r \leqslant H} \rho(H,H_r)\, dH dH_r = M_s. \tag{2}$$

But if a system contains a reversible component of the form $M_{rev}(H)$, then this component is reduced to zero by the mixed second derivative in Eq. (1). Thus, the contribution of $M_{rev}(H)$ will be missing from the integral, and the normalization condition in Eq. (2) will not be generally satisfied.

We next show that the FORC distribution can be given the desired normalization if we employ ''extended'' FORC's. As already mentioned, the set of FORC's, denoted by $M(H,H_r)$, is defined only for $H \geqslant H_r$, but we can mathematically extend $M(H,H_r)$ to the entire $\{H,H_r\}$ plane by defining

$$M^*(H,H_r) \equiv \begin{cases} M(H,H_r) & \text{if} \quad H > H_r \\ M(H=H_r,H_r) & \text{if} \quad H \leqslant H_r, \end{cases} \tag{3}$$

which can also be written as

$$M^*(H,H_r) \equiv \theta(H-H_r)M(H,H_r) + [1-\theta(H-H_r)]M(H=H_r,H_r), \tag{4}$$

where $\theta(x)$ equals 0 for $x \leqslant 0$ and 1 for $x > 0$. [Note that $1-\theta(x) \neq \theta(-x)$.] Then let us redefine the FORC distribution as

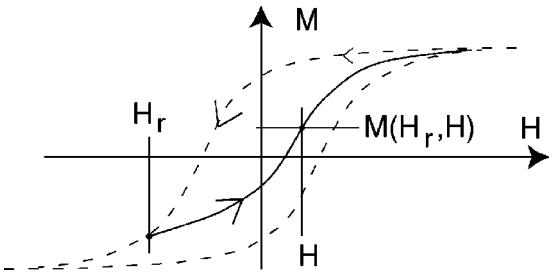

FIG. 1. A First-order reversal curve (FORC) is acquired after saturating the sample in a positive applied field. The applied field is lowered to a reversal field H_r. A FORC is the magnetization curve that results when the field is increased back to saturation. The magnetization at the applied field H on a FORC with reversal field H_r is denoted by $M(H,H_r)$.

$$\rho(H,H_r) \equiv -\frac{1}{2}\frac{\partial^2 M^*(H,H_r)}{\partial H_r \partial H}. \tag{5}$$

When the dataset is extended in this way, $\rho(H,H_r)$ is well defined for all $\{H,H_r\}$, and we have

$$\begin{aligned}
&\int\int \rho(H,H_r)\,dH\,dH_r \\
&= -\frac{1}{2}\int\int dH\,dH_r \frac{\partial^2 M^*(H,H_r)}{\partial H \partial H_r} \\
&= -\frac{1}{2}\int dH_r \frac{\partial}{\partial H_r}\left(\int dH \frac{\partial M^*(H,H_r)}{\partial H}\right) \\
&= -\frac{1}{2}\int dH_r \frac{\partial}{\partial H_r}[M_s - M(H=H_r,H_r)] \\
&= \frac{1}{2}\int dH_r \frac{\partial}{\partial H_r} M(H=H_r,H_r) \\
&= \frac{1}{2}[M_s - (-M_s)] = M_s,
\end{aligned} \tag{6}$$

which is the desired normalization.

In work with the Preisach model,[7] the contribution of the reversible component $M_{rev}(H)$ is sometimes included in the Preisach distribution by means of a δ function ridge on the $H=H_r$ axis equal to

$$\rho(H=H_r,H_r) = \frac{1}{2}\delta(H-H_r)\frac{dM_{rev}(H_r)}{dH_r}, \tag{7}$$

where $\delta(H-H_r)$ is the Dirac δ function. We next show that when we employ the extended FORC's just described, then the δ function in Eq. (7) arises as an integral part of the FORC distribution with the mixed second derivative in Eq. (1).

Let us evaluate $\rho(H,H_r)$ on the $H=H_r$ axis. We begin by taking the partial derivative with respect to H. We get

$$\begin{aligned}
\frac{\partial M^*(H,H_r)}{\partial H} &= \frac{\partial[\theta(H-H_r)M(H,H_r)]}{\partial H} \\
&\quad + \frac{\partial[(1-\theta(H-H_r))M(H=H_r,H_r)]}{\partial H} \\
&= \theta'(H-H_r)M(H,H_r) \\
&\quad + \theta(H-H_r)\frac{\partial M(H,H_r)}{\partial H} \\
&\quad - \theta'(H-H_r)M(H=H_r,H_r).
\end{aligned} \tag{8}$$

Since $\theta'(H-H_r)$ is zero everywhere except at $H=H_r$, then we can write

$$\theta'(H-H_r)M(H,H_r) = \theta'(H-H_r)M(H=H_r,H_r). \tag{9}$$

Thus, the first and last terms on the right-hand side of Eq. (8) cancel. If we take the partial derivative of Eq. (8) with respect to H_r, we get

$$\begin{aligned}
\frac{\partial^2 M^*(H,H_r)}{\partial H \partial H_r} &= -\theta'(H-H_r)\frac{\partial M(H,H_r)}{\partial H} \\
&\quad + \theta(H-H_r)\frac{\partial^2 M(H,H_r)}{\partial H \partial H_r}.
\end{aligned} \tag{10}$$

Since $\theta(H-H_r)$ equals zero when $H=H_r$, then the second term on the right-hand side of Eq. (10) evaluated on the $H=H_r$ axis equals zero. It can also be shown that

$$\begin{aligned}
&\left(\theta'(H-H_r)\frac{\partial M(H,H_r)}{\partial H}\right)\Big|_{H=H_r} \\
&\quad = \delta(H-H_r)\lim_{H\to H_r^+}\frac{\partial M(H,H_r)}{\partial H},
\end{aligned} \tag{11}$$

where the limit approaches from above. Hence, $\rho(H,H_r)$ evaluated on the $H=H_r$ axis becomes

$$\rho(H=H_r,H_r) = \frac{1}{2}\delta(H-H_r)\left(\lim_{H\to H_r^+}\frac{\partial M(H,H_r)}{\partial H}\right). \tag{12}$$

For a reversible magnetization of the form $M_{rev}(H)$, Eq. (12) is equivalent to Eq. (7). Hence, by extending the FORC's in accordance with Eq. (3), we obtain the δ function ridge in Eq. (7) as an integral part of the FORC distribution. However, it should be emphasized that the expression in Eq. (12) is more general than Eq. (7). Equation (7) requires that the reversible magnetization be of the simple form $M_{rev}(H)$. In other words, Eq. (7) requires that the reversible magnetization can be decoupled from the irreversible state of the system. But in most real systems, the reversible magnetization is actually coupled to the irreversible state of the system. In the following section, a specific example is presented to demonstrate how the reversible and irreversible magnetizations can be coupled. The point here is that Eq. (12) makes no assumption about the form of the reversible magnetization and is applicable even if the reversible and irreversible magnetizations are coupled.

The extended FORC's proposed here also remove a technical problem involving the calculation of the FORC distribution near the $H=H_r$ axis. In our work with FORC diagrams, we employ datasets where the reversal fields and the data points on each FORC are uniformly spaced.[1] Thus, on a field plot such as Fig. 2, a dataset will form a square grid. To calculate $\rho(H,H_r)$ at a point P, we do a local polynomial fit on a local square grid of data points centered about P, as illustrated in Fig. 2. Since the raw FORC data have no data points for $H<H_r$, this method becomes problematic as one approaches the $H=H_r$ axis. But with the extended dataset proposed here, the square grid of data points covers the entire plane. Hence, a local polynomial fit can be performed at all points in the $\{H,H_r\}$ plane.

Finally, for the purpose of plotting a FORC distribution, it is convenient to change coordinates from $\{H,H_r\}$ to $\{H_c=(H-H_r)/2,\ H_b=(H+H_r)/2\}$.[1] With this change of coordinates, the $H=H_r$ axis becomes the $H_c=0$ axis and Eq. (12) becomes

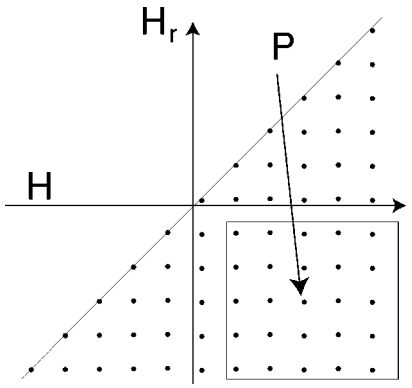

FIG. 2. On a field plot, each FORC is plotted on a horizontal line with vertical position equal to H_r. Each data point on a FORC appears at a horizontal coordinate equal to the applied field H at that data point. Our datasets make up a square grid on a field plot. An actual dataset would include thousands of data points. The FORC distribution at a point P is obtained with a local polynomial fit on a 5×5 square grid centered at P, as indicated above.

$$\rho(H_c=0,H_b)=\delta(H_c)\frac{1}{2}\left(\lim_{H\to H_r^+}\frac{\partial M(H,H_r)}{\partial H}\right)\Bigg|_{H_r=H_b}. \tag{13}$$

The derivative in Eq. (13) is just the reversible magnetization on the descending major hysteresis loop at applied field H_b. It should be noted that for $H<H_r$, or equivalently $H_c<0$, the FORC distribution is equal to zero.

III. DEMONSTRATION

We next demonstrate the application of these extended FORC datasets to experimental data with a sample of a Sony high-density floppy disk magnetic medium. The exact composition of this medium is proprietary, but the magnetic component consists of fine γ-Fe_2O_3 single-domain particles. The magnetization of the data has been normalized so that $M_s=1$. The FORC diagram for this sample is shown in Fig. 3(a), in the $\{H_c,H_b\}$ coordinates. In the contour shading legend, Max denotes the value of the FORC distribution at its ''irreversible'' peak (located at roughly $H_c=90$ mT). The ρ distribution goes to zero at the upper, bottom, and right hand boundaries of the FORC diagram. The shading at these boundaries corresponds to $\rho\approx0$ and shadings lighter than this represent negative regions of ρ, as indicated in the contour shading.

The FORC diagram in Fig. 3(a) shows a sharply peaked ridge on the $H_c=0$ axis. This ridge is just the δ function in Eq. (13), although it has been smoothed somewhat by the local polynomial fit described earlier. If the resolution of the dataset were increased, this ridge would approach a δ function. Since this ridge is due to the presence of reversible magnetization, we will refer to it as the ''reversible'' ridge. We should note that the high density of vertical contour lines near the $H_c=0$ axis in Fig. 3(a) makes the shading of the reversible ridge appear somewhat darker than it really is. The horizontal cross section at $H_b=-5$ mT in Fig. 3(b) gives a better measure of the magnitude of this ridge.

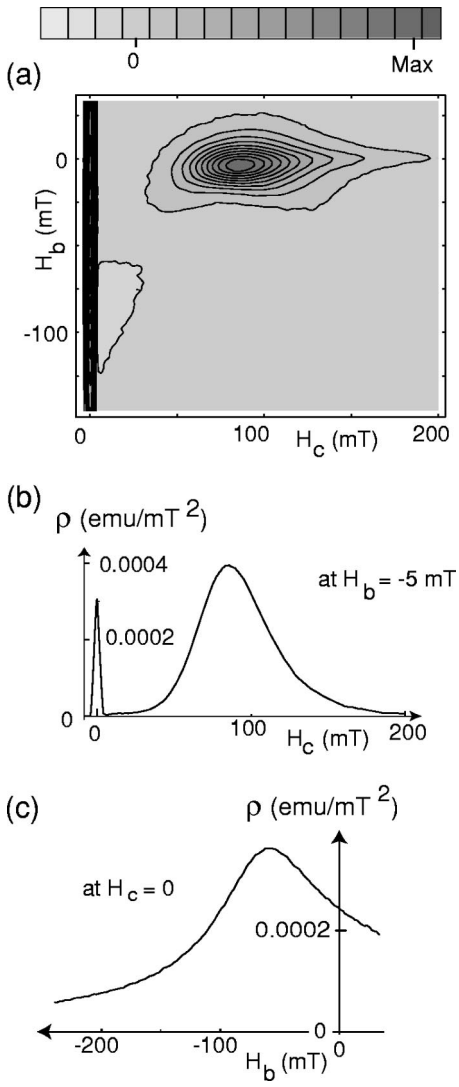

FIG. 3. (a) FORC diagram for Sony floppy disk sample, showing the reversible ridge at $H_c=0$. In the contour shading legend above the diagram, Max denotes the value of the FORC distribution at its ''irreversible'' peak (located at about $H_c=90$ mT). A negative region occurs adjacent to the vertical ($H_c=0$) axis at about $H_b=-85$ mT. Note that the high density of vertical contour lines near the $H_c=0$ axis makes the shading there appear darker than it really is. (b) A horizontal cross section passing though the irreversible peak at $H_b=-5$ mT. The ridge at $H_c=0$ can also be seen in this plot. (c) A vertical cross section through the reversible ridge at $H_c=0$.

The FORC diagram in Fig. 3 also shows two somewhat surprising features: If the system has a reversible magnetization of the form $M_{rev}(H)$, then $M_{rev}(H)$ should be an odd function of H and therefore the ridge should be a symmetric function of H_b. But the vertical cross section though the reversible ridge (at $H_c=0$) in Fig. 3(c) shows that the weight of the ridge as a function of H_b is nonsymmetric about $H_b=0$. A second surprising feature is a negative region in Fig. 3(a) adjacent to the vertical axis in the vicinity of $H_b=-85$ mT. To help us interpret these two features of the FORC diagram in Fig. 3, we next look at a simple model.

Let us begin our modeling work by defining the ''square''

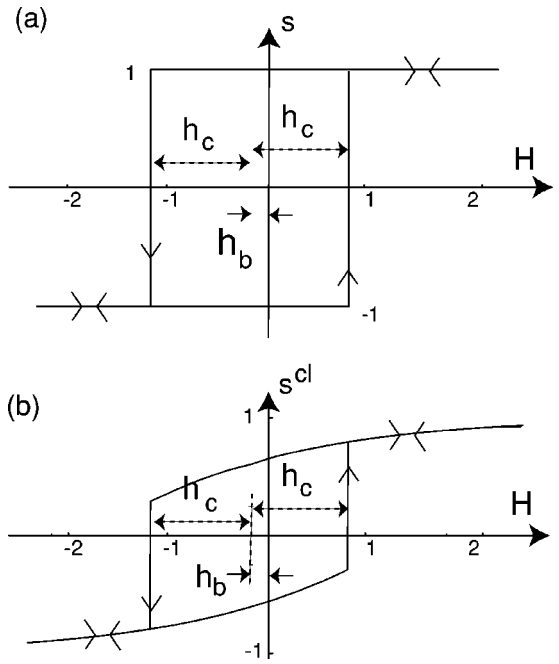

FIG. 4. (a) A basic hysteron s with coercivity h_c and bias h_b. (b) A curvilinear hysteron with the same h_c and h_b.

hysteron s illustrated in Fig. 4(a). The half-width and offset of s are referred to as its coercivity h_c and bias h_b, respectively. The value of s depends on the history of the applied field H in the following way: If the applied field begins at $H=\infty$, then s will start at $+1$ and will switch to -1 when H falls below $-h_c+h_b$, and will switch back to $+1$ when H rises above h_c+h_b. Next, let us add curvature to the top and bottom branches of s to obtain the "curvilinear" hysteron s^{cl} shown in Fig. 4(b). This curvilinear hysteron can be mathematically described by:

$$s^{cl} \equiv s\{1-g[s(H-h_b)/h_c)]\}, \tag{14}$$

where $s=\pm 1$ is the orientation of the square hysteron with coercivity $-h_c$ and bias $-h_c$, and where $g(H)$ must go to zero as H goes to infinity. Curvilinear hysterons of this type have been previously used in Refs. 7 and 8. For Fig. 4(b) and in our calculations we used

$$g(H)=2.34[\tanh(-0.34H-1.2)+1], \tag{15}$$

where this $g(H)$ was selected in order to fit the measured FORC diagram in Fig. 3, as we will see below.

Changes in magnetization coming from the curvature in Fig. 4(b) are reversible. But the slope, or susceptibility, of s^{cl} is not the same on the bottom and top branches. For example, just above $-h_c$, the top branch has a slightly larger susceptibility than does the lower branch. Therefore, the reversible magnetization of the curvilinear hysteron s^{cl} in Fig. 4(b) is coupled to its irreversible orientation. It cannot be expressed in the simple form $M_{rev}(H)$.

Let us consider a collection of N curvilinear hysterons with a distribution of coercivities and biases given by $P(h_c,h_b)=f(h_c)g(h_b)$. This distribution of bias is intended to represent a distribution of interaction fields in a collection

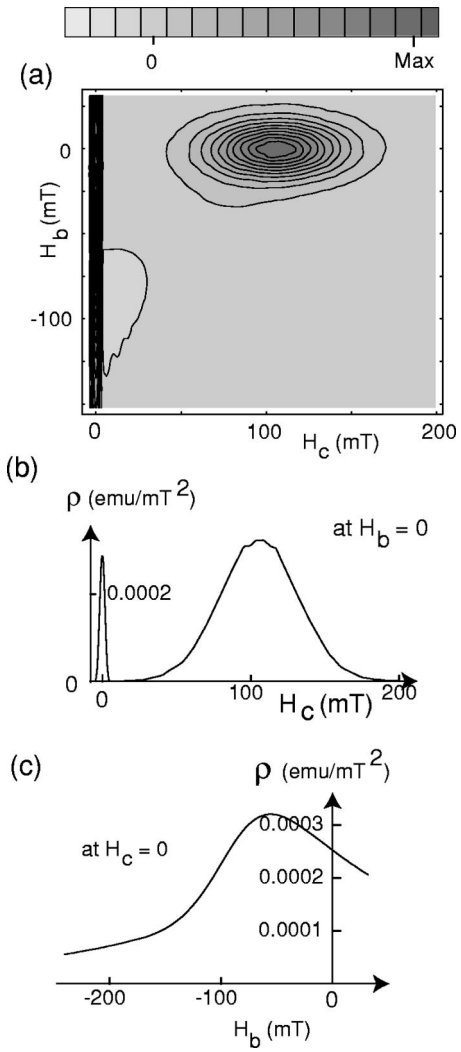

FIG. 5. (a) The FORC diagram of a collection of curvilinear hysterons, as described in the text. (b) A horizontal cross section through this FORC distribution at $H_b=0$. (c) A vertical cross section through the reversible ridge (i.e., at $H_c=0$).

of interacting particles. We will let $g(h_b)$ be a Gaussian with standard deviation 10.6, and $f(h_c)$ be a Gaussian with mean 106.4 and standard deviation 25.9, where these values are chosen to fit the data in Fig. 3. In our calculations, we let $N=400\,000$. The spacing of the fields in our numerical dataset is the same as the spacing in the experimental data (2.3 mT). The magnetization was normalized so that $M_s=1$. The FORC diagram for this collection of curvilinear hysterons is shown in Fig. 5(a).

As with the experimental data, the FORC diagram in Fig. 5(a) has a sharply peaked reversible ridge on the $H_c=0$ axis. The reversible ridge can also be seen in Fig. 5(b). In Fig. 5(c), we plot the vertical cross section though the reversible ridge (i.e., at $H_c=0$). As with the experimental data, this cross section is not symmetric about $H_b=0$. This lack of symmetry is due to the fact that, as discussed earlier, the upper and lower branches of the curvilinear hysteron in Fig. 4(b) do not have the same slope. In general, when the reversible magnetization is coupled to the irreversible state of the

system, as it is for this curvilinear hysteron, then the reversible ridge will be nonsymmetric about $H_b=0$.

The negative region of $\rho(H,H_r)$ in Fig. 5(a) is also due to the coupling between the reversible magnetization and the irreversible state of the system. To help understand how this negative region arises, consider this: When the hysteron in Fig. 4(b) switches down at $H_r=-h_c$, then its susceptibility at H just above $-h_c$ decreases, because the hysteron is now on its lower branch. So as H_r is lowered and passes through $H_r=-h_c$, the susceptibility of the FORC's at applied fields just above $H=-h_c$ can slightly decrease. If the susceptibility of the FORC's, at some fixed applied field H, decreases as H_r is lowered, then a negative value in the FORC distribution will result [see Eq. (1)].

As already noted, the distributions $g(h_b)$ and $f(h_c)$ in our model were chosen to fit our model to the data in Fig. 3(a). However, the features of the FORC diagram which are of interest here—the asymmetry of the reversible ridge and the presence of a negative region—are purely a consequence of the curvilinear hysteron in Fig. 4(b).

Finally, we note that the ''irreversible'' part of the FORC distribution in Fig. 3(a) has some interesting fine structure. At high H_c, the distribution has a ''tail'' along the horizontal ($H_b=0$) axis; and the distribution peak, at about $H_c=90$ mT, is located slightly below the $H_b=0$ axis. By contrast, the modeled distribution in Fig. 5(a) is simply the product of Gaussian coercivity and bias distributions. To obtain the same fine structure in our modeled FORC distribution would require a more realistic model of interactions than the one used here. In a future paper, we will discuss in detail the relationship between interactions and the tail in Fig. 3(a).

IV. CONCLUSION

A FORC diagram contains detailed information about the hysteresis behavior of a magnetic system. Currently, a number of workers are looking for ways to interpret and apply this information. In this paper, we have addressed three issues which have hindered the use of FORC diagrams. The extended FORC's proposed here enable a FORC diagram to fully capture the contribution of the reversible magnetization. They make the numerical calculation of the FORC distribution robust near the $H=H_r$ axis. And with these extended FORC's, the normalization of the FORC distribution is equal to the saturation magnetization.

[1] C. Pike, A. Roberts, and K. Verosub, J. Appl. Phys. **85**, 6660 (1999).
[2] C. Pike and A. Fernandez, J. Appl. Phys. **85**, 6668 (1999).
[3] H. Katzgraber, F. Pazmandi, C. Pike, K. Liu, R. Scalettar, V. Verosub, and G. Zimanyi, Phys. Rev. Lett. **89**, 257202 (2002).
[4] A. Muxworthy and D. Dunlop, Earth Planet. Sci. Lett. **203**, 369 (2002).
[5] A. Stancu, C.R. Pike, L. Stoleriu, P. Postolache, and D. Cimpoesu, J. Appl. Phys. **93**, 6620 (2003).
[6] I. Mayergoyz, IEEE Trans. Magn. **MAG-22**, 603 (1986).
[7] E. D. Torre, *Magnetic Hysteresis* (IEEE, New York, 1999).
[8] I. Mayergoyz, *Mathematical Models of Hysteresis* (Springer-Verlag, New York, 1991).